ATS-3 observed cloud brightness field related to a meso-to-subsynoptic scale rainfall pattern

By D. N. SIKDAR, *Space Science and Engineering Center, The University of Wisconsin, Madison, Wisconsin, U.S.A.*

(Manuscript received November 18, 1971)

ABSTRACT

The geosynchronous satellite (ATS-III) time lapse cloud brightness data have been analyzed with a view to correlating the time variations of cirrus shield area to rainfall rate in mid-latitude storm complexes. While inadequate rainfall sampling precludes point-to-point comparison, an excellent correlation is obtained with the time-change of radar echo areas in the cloud complex. Also presented are preliminary results on excellent correspondence between subsynoptic scale cloud brightness anomaly patterns and the precipitation patterns in mid-latitude frontal zones.

1. Introduction

In the past decade there has been a growing interest in the use of meteorological satellite data with a view to an elucidation of the pattern and processes of meteorological events for ultimate use in the long-range weather prediction model. Two University of Wisconsin experiments, Spin scan cameras on board the ATS-I and ATS-III satellites, have further stimulated efforts toward that goal. ATS (Applications Technology Satellite) time-lapse information has been used in the remote sensing of the dynamics and energetics of convective systems across a wide range of space and time scales (Sikdar & Suomi, 1971; Sikdar et al., 1970). Precipitation plays a significant role in storm energetics, through interaction with the airflow, yet on many occasions, because of its mesoscale nature, it escapes detection by the generally sparse network of raingauge stations. The use of satellites in determining rainfall on a large scale therefore has obvious advantages over rainfall measurements made at points on the earth's surface.

In the recent past, a number of investigators have had some success in relating rainfall to data obtained from earth-orbiting satellites (Gerrish, 1970; Barrett, 1970; Rainbird, 1969). The primary objective of this study is to investigate the degree of correspondence between ATS-observed cloud features and characteristics on a meso-to-subsynoptic scale, and rainfall patterns. It is hypothesized that cloud particles in the cirrus canopy come from the penetrating towers and are distributed laterally by the upper wind field. This lateral spread is related to the divergence at the upper level (Sikdar, 1969) which in turn is related to the number of active cumulonimbi entering the shield and to their updraft velocity. Rainfall rate in a thunderstorm complex has a unique relation to the vertical motion field; therefore, it should have a good correspondence with the cirrus shield area change. This conjecture will be examined in the two mesoscale analyses presented in this paper.

The study area and the data source for this case study are the same as those already presented by Sikdar et al. (1970) except for the subsynoptic scale analysis. The presentation has been divided into two sections: the first dealing with the comparisons of the meso-scale rainfall pattern with cirrus shield area expansion atop deep convective systems; the second dealing with the comparison of subsynoptic scale isohyet patterns with cloud brightness anomaly patterns.

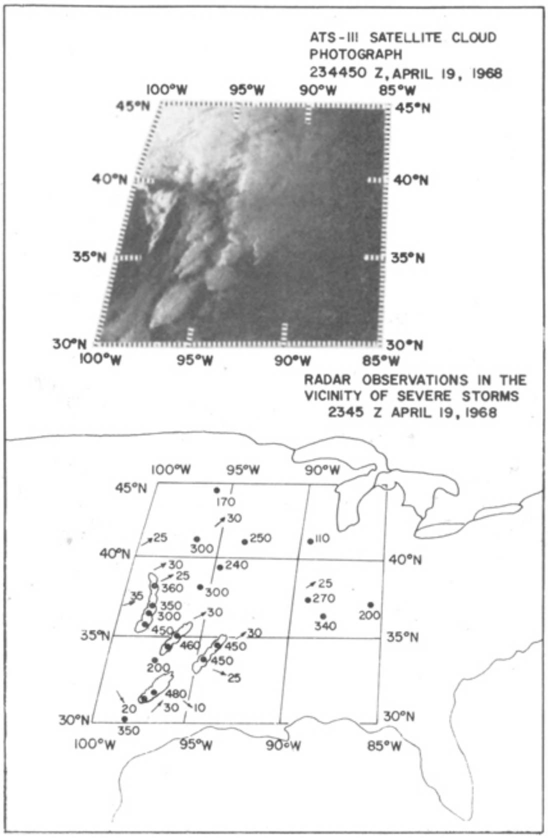

Fig. 1. (*a*) A section of ATS-111 cloud photograph on 19 April 1968 showing the area of severe storm clouds at 234450 GMT. (*b*) Radar echoes at 2345 GMT in the vicinity of severe storm on 19 April 1968.

2. ATS-observed convective cloud features and the synoptic situation in the study area

Fig. 1*a* is a section of ATS-III cloud photographs at 234450 GMT on 19 April 1968. The most spectacular feature in this picture is the presence of cirrus outflow from convective towers in the dry environment marked by a clear space. A careful examination of the cloud complexes on high quality photographs reveals the presence of bright spots, probably resulting from towers penetrating the cirrus shield. The majority of those bright spots are aligned north-south along the 97° W meridian with a second such front along the 94° W meridian.

Fig. 1*b* presents radar echoes located in the region of confluence between moist air streaming northward from the Gulf of Mexico and dry air moving from the west. The region of storm development was characterized by a high-level jet overrunning the axis of low-level moisture inflow, a typical synoptic situation favoring severe storm development (Fawbush et al., 1951; Fawbush & Miller, 1953).

Fig. 2 is another example exhibiting similar meso-scale cloud characteristics on 23 April 1968. Thunderstorm activity became pronounced between 1900 to 2200 GMT and continued late into the night of the 23rd.

In regard to subsynoptic scale analysis, the reader is referred to cloud features east of longitude 94°W in Fig. 1. A massive cirrus canopy emerging from a few scattered thunderstorm complexes extends north–south, with the cirrus outflow aligned SW to NE. In contrast to the meso-scale regime along the 97° W meridian, hardly any clear space around any individual thunderstorm complex can be identified in this region. This renders isolation of an

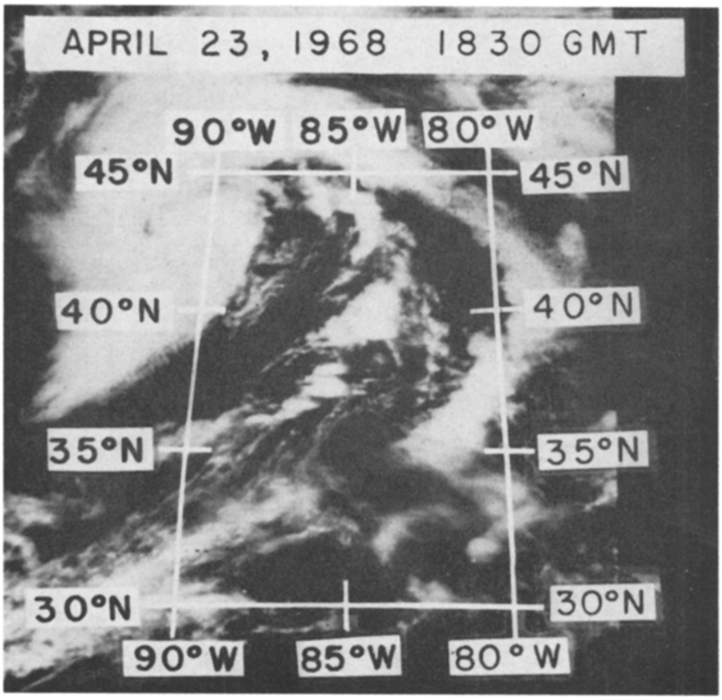

Fig. 2. Same as in Fig. 1*a* but for 23 April 1968 at 1830 GMT.

individual complex difficult, although a relative cloud brightness gradient is noticed in the area 92° W–94° W, 37° N–40° N and 92° W–95° W, 33° N–37° N.

3. Data processing

a. *Meso-scale*

The grid matrix of ATS-III cloud photos consists of 8196 digital elements and 2018 west to east scan lines. Within this grid we have information ranging from 0 to 255 digital counts. Meso-scale convective systems, while difficult to analyze on photographic images because of the photographic image's limited dynamic range, can easily be treated on brightness-normalized digital contour displays.

Satellite picture normalization involves two important steps: (1) navigation, and (2) brightness correction for sun-satellite-cloud geometry. Some complications in cloud brightness normalization are obvious, for the cloud brightness depends on many variables, including solar zenith angle, satellite viewing angle, the location of the cloud with respect to the sun and satellite, and camera response characteristics. The most important of them is the dependence on solar zenith angle, if one neglects attenuation and scattering by the atmosphere and assumes uniform performance of camera and recording systems. Although clouds in general are not Lambertian reflectors (Ruff et al. 1967), over limited geometries on the scale of resolution of the ATS camera thick cirrus shields emerging from cumulonimbus towers do tend to behave as such reflectors (Martin & Suomi, 1971). Accordingly, for deep convection regimes in satellite photos, our major interest in this paper, we have normalized cloud brightness for cosine angle change only.

Sample photographs of computer processed normalized iso-contour brightness displays of cloud systems in Figs. 1 and 2 are shown in Figs. 3 and 4. For correlating rainfall rate with the cirrus shield area-change, hourly precipitation charts were prepared for meso-systems having lifetimes much longer than two hours. The raingauges that received rainfall from a particular cloud system were identified by superimposing a number of brightness contour displays, made 28 minutes apart, on

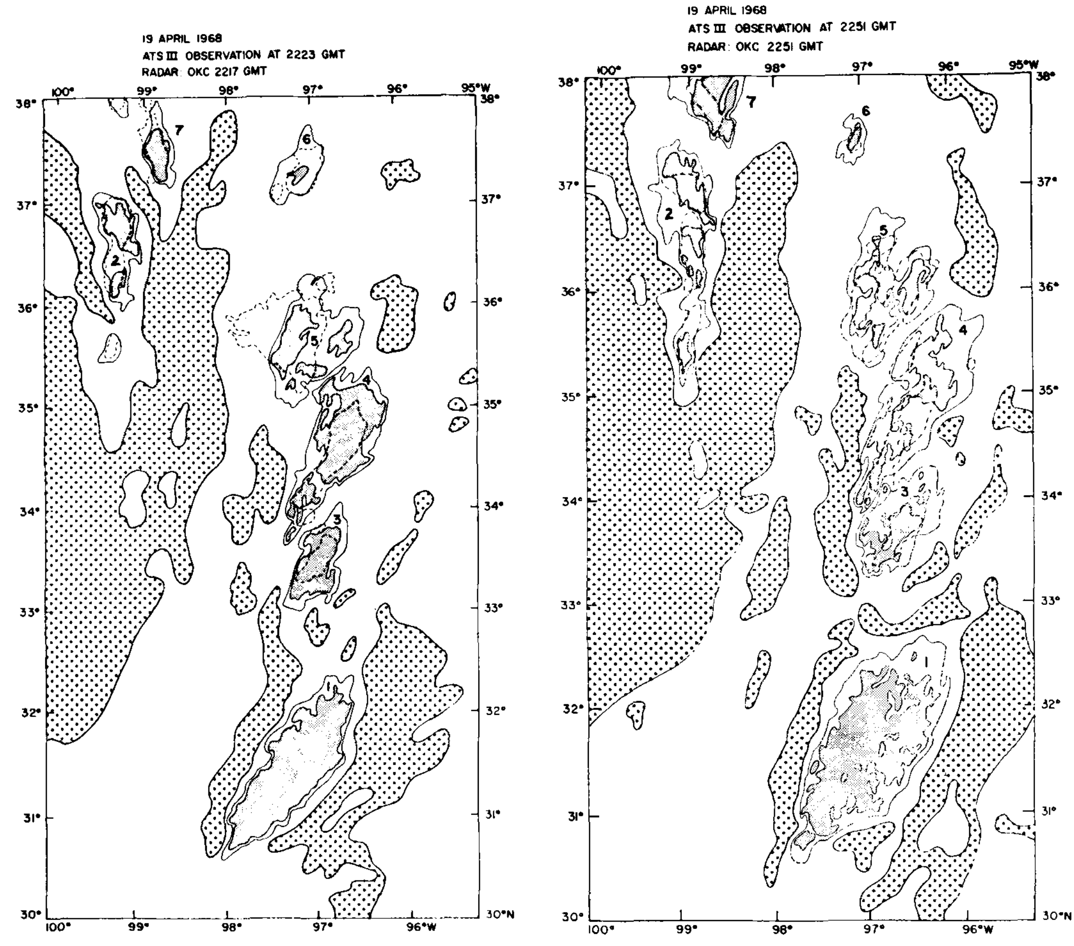

a b

Fig. 3a, b. ATS-111 observations at 2223 and 2251 GMT on which are superimposed radar observations from OKC at 2217 and 2251 GMT respectively. Clear areas are stippled. Thin cloud outlines represent upper 40 % of the total brightness range in the picture while the shaded areas are 30 %. Radar echoes are outlined by broken lines.

the precipitation charts and also by considering radar echo displacements during the hour. The areas of high cloud-brightness (approximately the uppermost 20 % of the ATS total-brightness range in the grid) were assumed to be the core region and the primary sources of precipitation.

Hourly precipitation data were analyzed and, in addition, a number of radar images were enlarged for comparison with near-simultaneous ATS data. Radar data selection was governed by the availability of good quality radar pictures corresponding to the ATS digital tapes analyzed. Direct comparisons of ATS data with radar images were not possible because of projection differences. Therefore ATS data were converted to a gnomonic projection, with the nearest radar site as the origin, and displayed as contour maps of digital brightness on approximately the same scale as the enlarged radar pictures. Lack of point-to-point correspondence in the modified projections may be attributed to error sources such as distortion in the original ATS and radar data, measurement errors in determining the scale, enlargement inaccuracy, uncertainty in finding the exact location of radar sites on the ATS brightness displays and time differences between radar and satellite images. Time variations of normalized

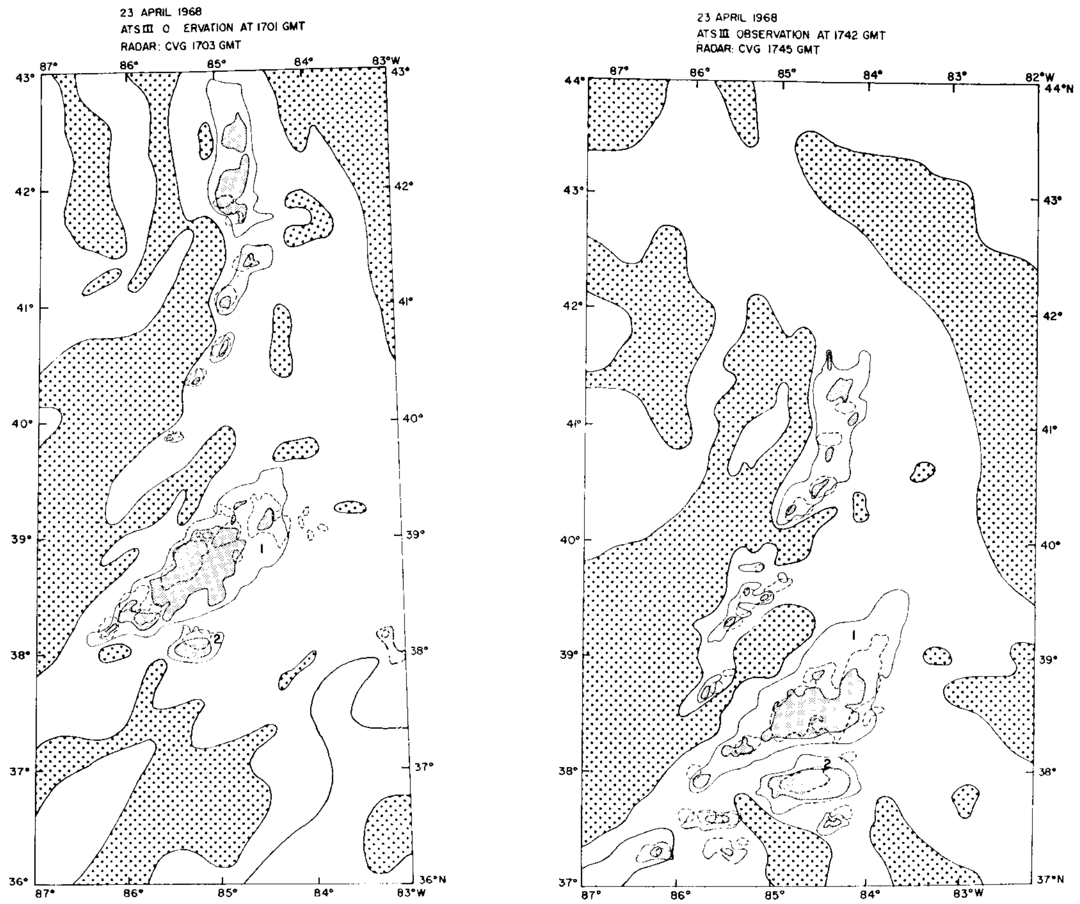

a b

Fig. 4a, b. Same as in Fig. 3 but for 23 April 1968. Thin cloud lines represent 36 % while the shaded areas are 22 %.

radar echo-areas were then compared with the cirrus shield-area expansion at intervals of 28 minutes. In matching the radar echoes with the brightness contour display, all radar echoes in cloud complexes were included in the upper 40 % of the ATS-III brightness range on the 19th, and the upper 36 % on the 23rd. This difference in cut-off level may be due to differences in geographic locations of the storm systems and also to differences in storm intensity. Fig. 5 is an example showing time variations of percent area of three contour levels (upper 22 %, 29 % and 36 % of the total brightness range in the grid) on the 23 April 1968. The purpose of this diagram is to show a uniform quasi-linear growth rate in all contour levels except in the last period when variation hardly exceeded a few percent in the 22 % contour area. This departure may be related to precipitation release in the core area after 1900 GMT, a fact actually observed beneath the cloud systems.

b. *Subsynoptic scale*

Navigated and brightness-normalized tapes were processed for the area 91° W–96° W and 33° N–41° N, as shown in Fig. 10. Each data point represents an average brightness of a small matrix of 10 scan lines × 33 elements (size approximately 1/2° latitude × 1/2° longitude). Brightness anomaly ($B_a = B_{i,j} - \overline{B}_j$, $i = 1, 113$, $j = 1, 3$, where i = number of small grid boxes; j = number of pictures used) charts were constructed in Eulerian coordinate for pictures

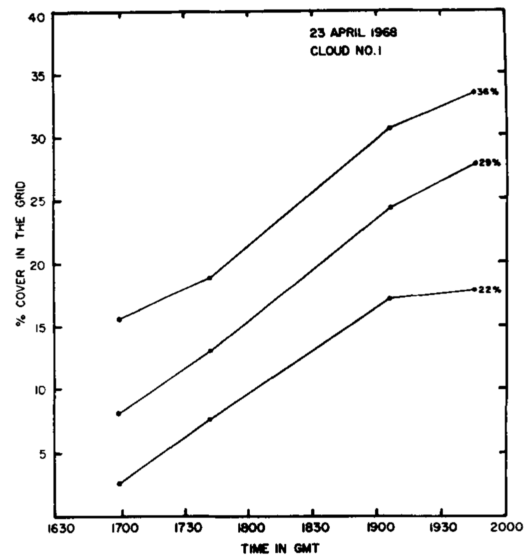

Fig. 5. Time variations of percent cover in the grid of brightness contour of upper 36, 29, and 22 % of total brightness range.

at 2156, 2223 and 2251 GMT, and isocontours were drawn. Hourly precipitation charts were made for the same area, ending at 2200, 2300 and 2400, and the patterns of isohyets drawn. Although inadequate rainfall sampling prohibits one-to-one comparison, it was felt that some useful information could be derived on the feasibility of estimating rainfall patterns from the ATS time-lapse information, especially for areas of ill-defined convective cloud regimes. To increase confidence in the objectivity of the technique, radar echoes from Kansas City and Little Rock, properly normalized for the ATS scale, are superimposed on the brightness anomaly displays.

4. Results

a. *Correlation between cirrus shield area change and rainfall rate*

Fig. 6 is a map of hourly precipitation ending at 2300 GMT upon which is superimposed the cloud brightness contour at 2223 GMT outlining the upper 40 % of the total brightness range in the picture. Inadequancy of raingauge density for meso-scale analysis is apparent from this diagram. Hourly rainfall data from various raingauges in the path of the cloud complex during the hour, using technique outlined in section 3, are given in Table 1. The plots of these hourly rainfall averages and cirrus shield areas as a function of time for clouds number 1, 3 and 5 on 19 April 1968 and for 1 on 23 April 1968 are presented in Fig. 7. Selection of clouds was governed by the spatial rainfall sampling. Despite poor sampling in the complex, the trends in Fig. 7 indicate a definite positive correspondence between the outflow-area and the average rainfall amount. In case of cloud number 1 on 23 April 1968, most of the precipitation appears to have occurred in the late evening when no useable satellite observations were available because of darkness. However,

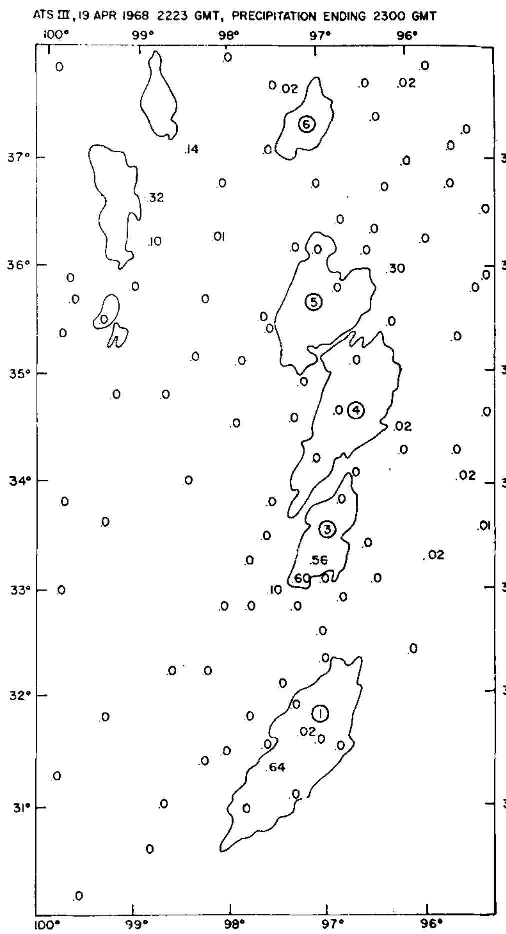

Fig. 6. Hourly precipitation (inches) chart ending at 2300 GMT superimposed on which is the upper 40 % brightness contour at 2223 GMT. Cloud numbers are circled.

Table 1. *Raingauge locations and hourly rainfall amount*

Time GMT	Reporting stations	Latitude North	Longitude West	Hourly rainfall in inches	Average rainfall
Date: 19 April 1968					
Cloud number 1					
2000–2100	Briggs	30°53′	97°55′	0.42	
	Moline	31°23′	98°19′	0.07	0.17
	Whitney Dam	31°52′	97°22′	0.01	
2100–2200	Coryell City	31°33′	97°37′	0.66	
	Evant	31°29′	98°04′	0.04	0.24
	Moline	31°23′	98°19′	0.03	
2200–2300	Waco WBAP	31°37′	97°15′	0.02	0.33
	Flat	31°19′	97°38′	0.64	
2300–2400	Rusil	31°29′	96°53′	0.39	
	Waco Dam	31°35′	97°06′	0.42	0.36
	Waco WB AP	31°37′	97°13′	0.28	
Cloud number 3					
2100–2200	Weatherferd	32°46′	97°49′	0.11	0.30
	Reno	32°57′	97°35′	0.5	
2200–2300	Justin	33°02′	97°19′	0.6	0.58
	Denton	33°13′	97°08′	0.56	
2300–2400	Gordonvelle	33°48′	96°51′	0.64	
	Ardmore Water-works	34°10′	97°08′	0.1	0.37
Cloud number 5					
2100–2200	Okema	35°26′	96°18′	0.01	0.01
2200–2300	Heyburn Dam	35°57′	96°17′	0.30	0.16
	Lehigh	34°28′	96°13′	0.02	
2300–2400	Heyburn Dam	35°57′	96°17′	0.07	0.07
Date: 23 April, 1968					
Cloud number 1					
1800–1900	Versailles Waterworks Indiana	39°05′	85°15′	0.18	0.18
1900–2000	London Sewage Plant, Ohio	39°53′	83°27′	0.90	
	Springfield New Waterworks Ohio	39°59′	83°49′	0.89	
	Lebanon HWY Dept. Ohio	39°26′	84°12′	0.84	0.68
	Xenia treatment plant	39°42′	83°54′	0.75	
	Covington WB Airport, Kentucky	39°04′	84°40′	0.22	

for studying a point-to-point correspondence both in space and time one needs detailed simultaneous aircraft and surface data on both variables. Unfortunately such simultaneous quantitative measurements were not available to us, except from a few closeby radar stations which photographed the PPI scope.

Before we discuss radar echoes related to cirrus shield expansion it is worthwhile to plot the time change of the cirrus shield area against the rainfall amount obtained from Fig. 7 (Fig. 8). The data interval picked up from Fig. 7 for comparison are indicated at the bottom of each inset. Although there is some scatter in

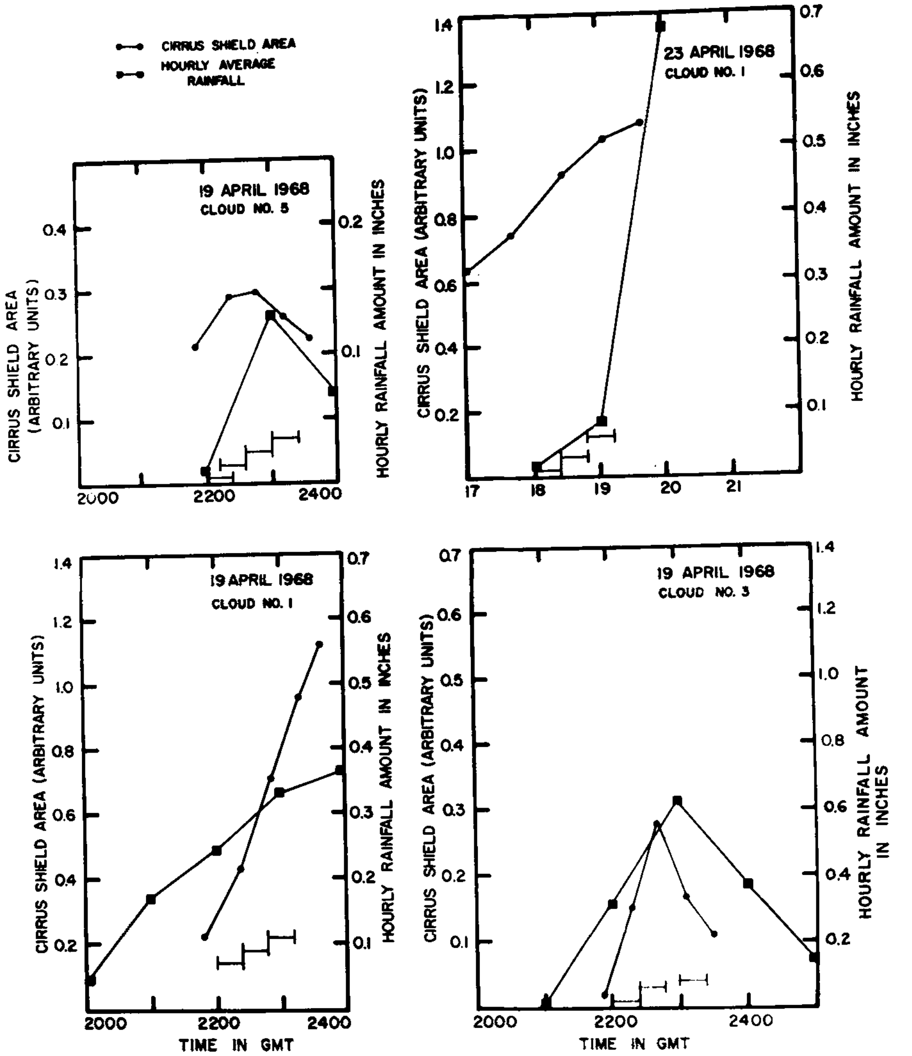

Fig. 7. Time variation of cirrus shield area and cumulative hourly precipitation on 19th and 23rd in storm complexes investigated.

the data points in Fig. 8, a general agreement between the two variables is apparent. Most interesting in this data set is cloud number 1 on 19 April 1968 which showed significant outgrowth but produced comparatively little precipitation. Lack of meteorological data incloud and in the immediate environment at the time of storm-growth precludes any definite explanation for this phenomenon. It is however possible that a major part of the water vapor entering into the storm have passed on to ice phase due to strong updraft and escaped precipitation and also that, a part of the precipitation in the downdraft might have evaporated in the dry environment before reaching the ground. These two effects together can account for such a phenomenon. In fact, the upper air soundings in the synoptic scale environment prior to the occurrence of the storm do suggest a dry condition in the inflow layer with a strong inversion at about 915 mb. Unfortunately, no suitable time sequence of radar observations were available to verify the time-change in precipitation area beneath this cloud.

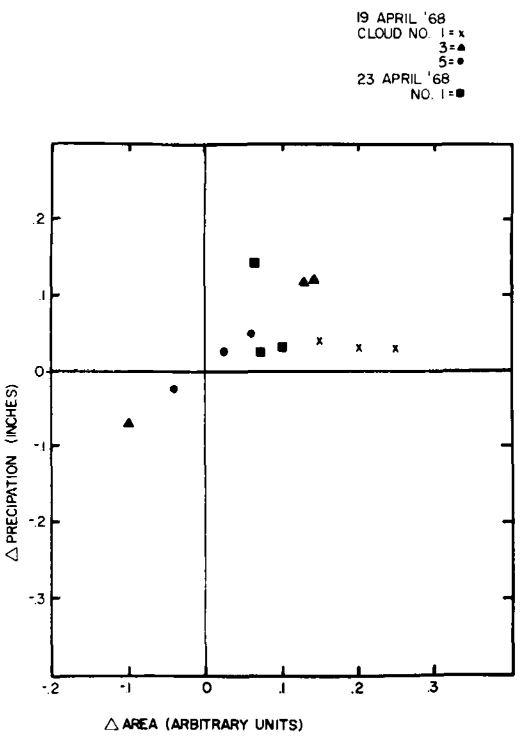

Fig. 8. Correlation between the cirrus shield area change and the change in the hourly precipitation amount as derived from Fig. 7.

To examine the degree of correspondence more closely we have used time variations of radar echo area in respective cloud complexes (Figs. 3, 4). We have assumed that the radar echo area change is a measure of change in vertical motion field and therefore a change in rainfall rate during the life cycle of the complex. No normalization of the radar echo areas was attempted except for matching the ATS scale, for we were mainly concerned with the relative changes in the echo-area in 28 minutes. In this time interval, the clouds had hardly moved more than 10–15 n.m. Radar photos from Oklahoma City were employed for the case studies on the 19th and from Cincinnati and Detroit for 23rd. We limited our comparison to within 100 n.m. except for cloud number 3 on April 19, which was around 125 n.m. from the OKC radar site. In making comparisons, only those severe storm clouds that could be identified as individual complexes were selected. In Figs. 3 and 4 radar echoes have been superimposed on near-simultaneous satellite pictures. A comparison of solid radar echo area and the area of bright portions of the ATS images (the uppermost 36 % to 40 % of the total brightness range in the picture) in general yielded a good correspondence except for a few small scattered echoes which had no cloud counterpart above the selected brightness cut off level. However, most of these small echoes corresponded to the brightness cut off level at the upper 50 %–60 % of the total range in the pictures.

Fig. 9 presents the plot of the radar echo area-change against cirrus shield area-change. A good correlation is apparent in this data sample. Although this data sample is too small, it appears that an echo area change of one corresponds to a cirrus area change of three.

b. *Correlation between subsynoptic scale rainfall pattern and ATS cloud brightness anomaly pattern*

Presented in Fig. 10 are brightness anomaly charts at 2156, 2223 and 2251, and hourly rainfall distribution in the same area ending at 2200, 2300 and 0000 (20 April 1968) GMT east of 96° W (Fig. 1). A time change in the brightness anomaly field observed in this figure may be attributed to decreasing mean brightness values (Table 2) as the disturbance moved eastward through the fixed grid box which resulted in a greater clear area caused by advected dry air from the west. A higher convective activity during the same period resulted in an increase in percent cover of high brightness values (e.g. the area contoured by the

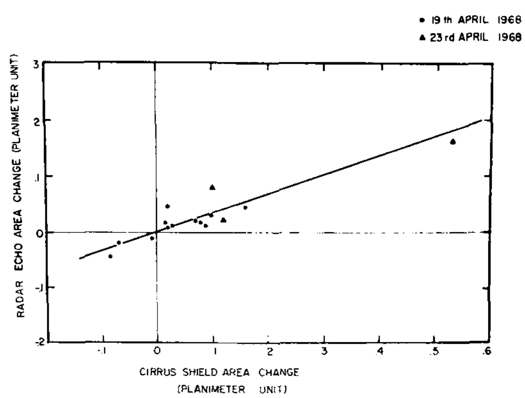

Fig. 9. Time variation of cirrus shield area against that of radar echo area in various storm complexes.

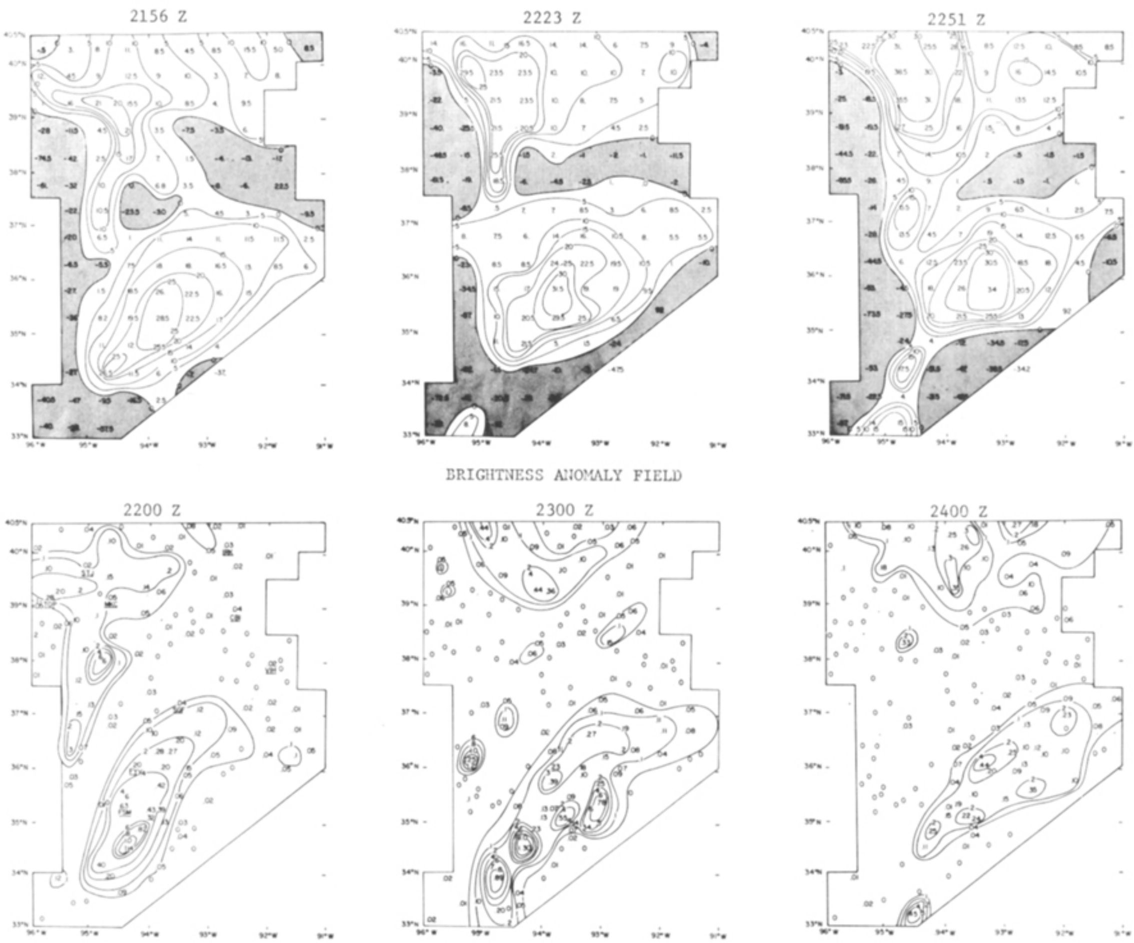

ISOHYETS OF RAINFALL

Fig. 10. Upper diagrams are ATS observed subsynoptic scale brightness anomaly field (negative anomaly fields are shaded) at 2156, 2223 and 2251 on the 19th while bottom diagrams show hourly rainfall charts ending at 2200, 2300, and 2400 GMT in the same area.

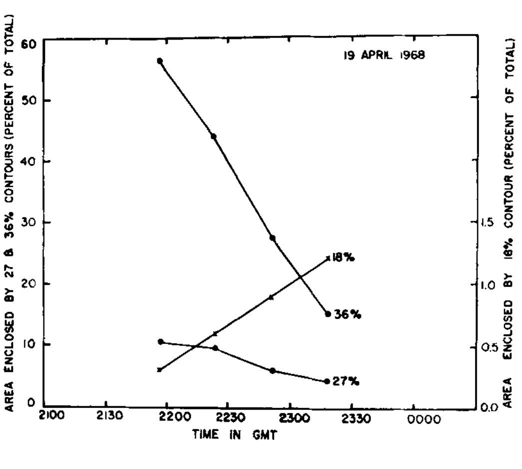

Fig. 11. Time variation of area enclosed by 18, 27, 36 % contour (percent of total) in the area as in Fig. 10.

upper 18 % in Fig. 11 increased with time). The increased convective activity and greater precipitation intensity and extent are borne out clearly in the time section. Although space averaging suppressed a few meso-scale rainfall areas in the brightness anomaly chart, a striking agreement was found between the subsynoptic scale brightness anomaly field at 2156, 2256 GMT and the hourly rainfall pattern ending at 2200 and 2300 GMT respectively. To substantiate objectivity in drawing isohyet

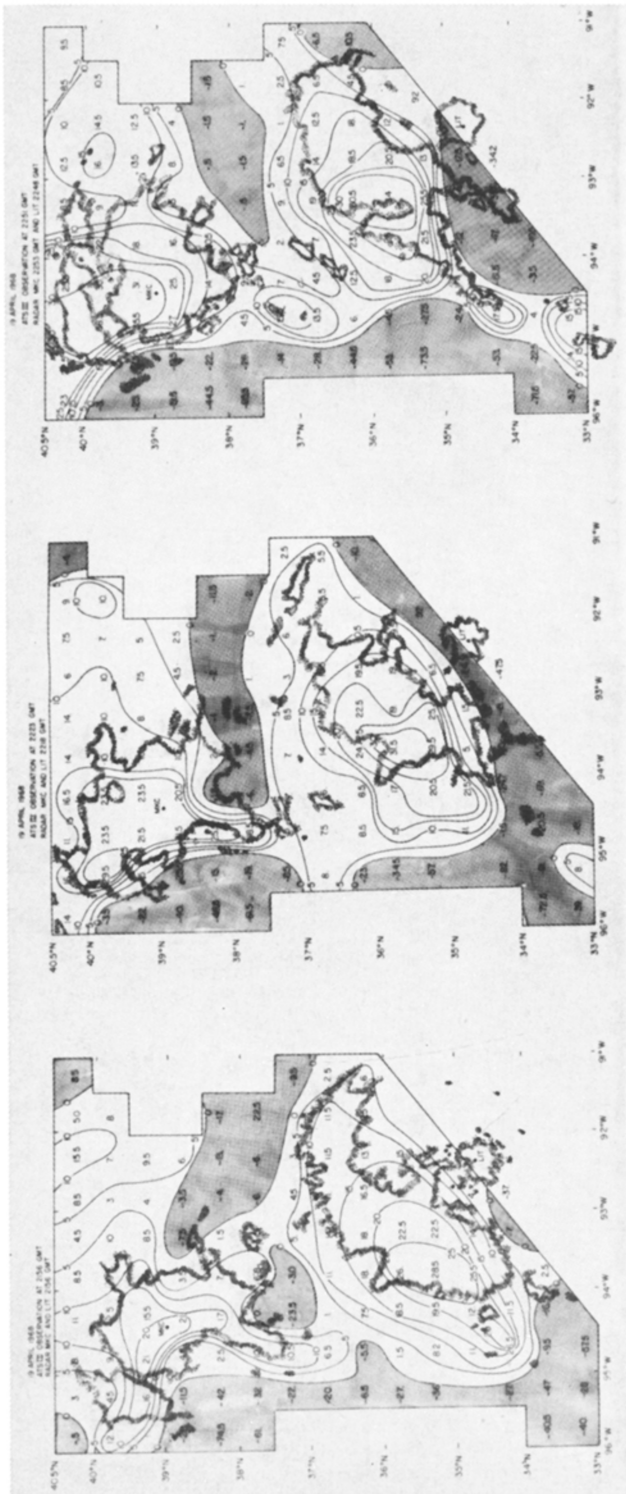

Fig. 12. Superimposition of near simultaneous radar echoes from Kansas City and Little Rock on the brightness anomaly fields in Fig. 10.

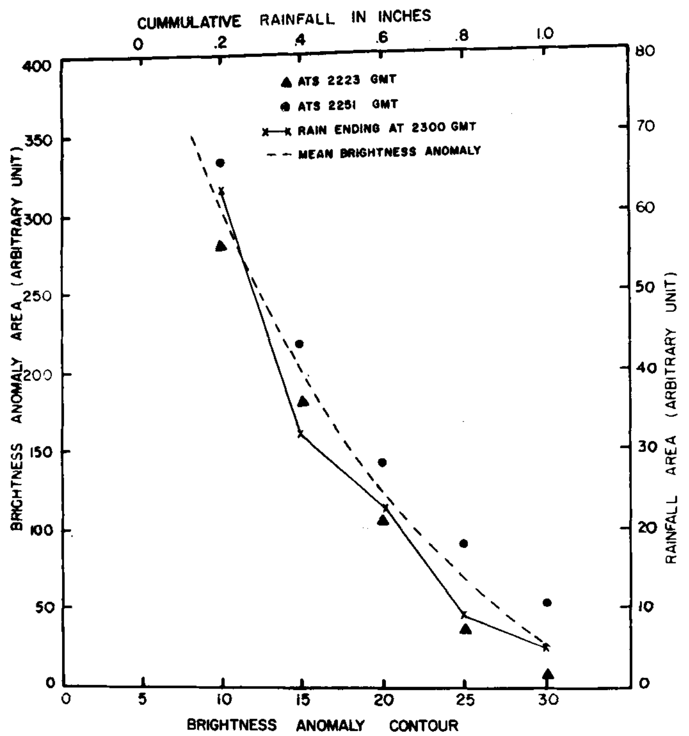

Fig. 13. Plots of brightness anomaly area and cumulative hourly rainfall area against brightness anomaly contour and isohyets of rainfall respectively as derived from Fig. 10.

patterns on the hourly rainfall charts, near simultaneous radar echoes from Kansas City and Little Rock have been superimposed on the brightness anomaly displays (Fig. 12). A striking similarity between the isohyet pattern and the radar echo distribution is revealed in this diagram.

In summary, there is an excellent correlation between the positive brightness anomaly area, radar echo area and the precipitation pattern. For more quantitative information on the correspondence, measurements on brightness anomaly area were taken from the average of two charts at 2156 and 2223 GMT (Fig. 10) and corresponding rainfall area from the precipitation chart ending at 2300 hour GMT (Fig. 10) and plotted in Fig. 13. Cumulative hourly precipitation of less than 0.2 inches has been ignored in this plot. Table 3 presents the correlation between rain area and brightness anomaly area as read out from Fig. 13.

Table 2. *Time variation of mean brightness*

Time (GMT)	Mean brightness ($\bar{B}$) (digital number)
2 156	183.6
2 223	177.4
2 251	166.0

5. Concluding remarks

Although the data sample presented in this research is small they have shown clearly a good correspondence between rainfall rate and time change of cirrus shield area atop active deep convection in mid-latitude frontal zones. Also seen from the superposition of normalized ATS brightness iso-contours on properly scaled radar photographs is a good agreement between the occurrence of rain at the ground and the absolute brightness of cloud masses. High absolute brightness of a cloud mass, however,

Table 3. *Correlation between rain area and brightness anomaly area as read from Fig. 13.* 1 arbitrary unit = ¼ (deg)² approximately

Brightness anomaly area (arbitrary unit)	Rain area (arbitrary unit)	Cumulative hourly rainfall in inches
310	63	0.2
250	47	0.3
200	36	0.4
160	29	0.5
125	22	0.6
90	16	0.7
50	11	0.8
45	7	0.9
30	3	1.0

may not be a sufficient criterion for assessing the intensity and stage of activity of cumulonimbus cells beneath it.

Furthermore, in the subsynoptic disturbance regime where extensive thick cirrus canopy and low clouds preclude visual isolation of individual complexes, brightness anomaly patterns are very helpful. Areas of a positive brightness anomaly pattern seem to agree well with isohyet patterns on the hourly rainfall chart. However, for a more useful time sequence, such charts should be constructed in Lagrangian coordinate rather than in Eulerian system so that the mean brightness can be weighted over the moving cloud systems only.

It may be reasonably concluded from this research that remote sensing of intensity, extent and frequency of meso-to-subsynoptic scale convective precipitation is possible from a geostationary altitude. Further study in this area should be fruitful from the viewpoint of synoptic meteorology and climatology.

Acknowledgements

The research reported in this paper was supported by the National Aeronautics and Space Administration under contract number NAS-5-11542. The author is thankful to Dr D. W. Martin for reviewing the manuscript and to Professor V. E. Suomi for constant encouragement and valuable discussion during the course of this work. Thanks are due to many individuals at the Space Science and Engineering Center for contributing in many ways in this research program.

REFERENCES

Barrett, E. C. 1970. The estimation of monthly rainfall from satellite. *Mon. W. Rev. 98*, 4, 322–327.

Fawbush, E. J., Miller, R. C. & Starrett, L. G. 1951. An empirical method of forecasting tornado development. *Bull. Amer. Meteor. Soc. 32*, 1–9.

Fawbush, E. J. & Miller, R. C. 1953. The tornado situation of 17 March 1951. *Bull. Amer. Meteor. Soc. 34*, 139–145.

Gerrish, H. P. 1970. Satellite and radar analysis of meso-scale features in the tropics. *Semi-annual report, ECOM-0205-20*, U.S. Army Electronics Command, Fort Mammouth, New Jersey.

Martin, D. W. & Suomi, V. E. 1971. A satellite study of cloud clusters over the tropical North Atlantic Ocean. *Final report on STAG contract E-127-69-(N)*, NOAA.

Rainbird, A. F. 1969. Some potential applications of meteorological satellites in flood forecasting. *Hydrological Forecasting*, WMO publication, No. 228, TP. 122, 73–80.

Ruff, I., Koffler, R., Fritz, S., Winston, J. S. & Rao, P. K. 1967. Angular distribution of solar radiation reflected from clouds as determined by TIROS radiometer measurements. *ESSA Tech. Report NESC-38*, U.S. Dept. of Commerce, Washington, D.C.

Sikdar, D. N. 1969. Convective heat transport over the tropical mid-Pacific as estimated from a geosynchronous satellite altitude. Ph.D. thesis, Dept. of Meteorology, The University of Wisconsin, Madison.

Sikdar, D. N., Suomi, V. E. & Anderson, C. E. 1970. Convective transport of mass and energy in severe storms over the USA. An estimate from a geostationary altitude. *Tellus 22*, 5, 521–532.

Sikdar, D. N. & Suomi, V. E. 1971. Time variation of tropical energetics as viewed from a geostrationary altitude. *Jour. Atmos. Sci. 28*, 2, 170–180.

СВЯЗЬ ЯРКОСТИ ОБЛАКОВ ПО ДАННЫМ АТС-3 С МЕЗО- И СУБСИНОПТИЧЕСКИМИ ПОЛЯМИ ОСАДКОВ

Изменения со временем яркости облаков по данным геосинхронного спутника (АТС-III) проанализированы с точки зрения корреляции временных изменений покрова циррусов со скоростью выпадения осадков в вихревых образованиях средних широт. Хотя ненадежные данные по осадкам не допускают поточечного сравнения, нами получена отличная корреляция с изменением во времени областей радерного эхо в облачном комплексе. Представлены также результаты по замечательному соответствию между анамальной яркостью облаков субсиноптического масштаба и осадками во фронтальных зонах средних широт.